NASA
Technical Memorandum 86881

USAAVSCOM
Technical Report 84-C-19

Experimental and Analytical Study of Ceramic-Coated Turbine-Tip Shroud Seals for Small Turbine Engines

T.J. Biesiadny, G.E. McDonald,
R.C. Hendricks, and J.K. Little
Lewis Research Center
Cleveland, Ohio

R.A. Robinson and G.A. Klann
Propulsion Laboratory
AVSCOM Research and Technology Laboratories
Lewis Research Center
Cleveland, Ohio

and

Eliot Lassow
Howmet Turbine Components Corporation
Whitehall, Michigan

January 1985

EXPERIMENTAL AND ANALYTICAL STUDY OF CERAMIC-COATED TURBINE-TIP SHROUD SEALS FOR SMALL TURBINE ENGINES

T.J. Biesiadny, G.E. McDonald, R.C. Hendricks, and J.K. Little,
National Aeronautics and Space Administration
Lewis Research Center
Cleveland, Ohio

R.A. Robinson and G.A. Klann
Propulsion Laboratory
AVSCOM Research and Technology Laboratories
Lewis Research Center
Cleveland, Ohio

and

Eliot Lassow
Howmet Turbine Components Corporation
Whitehall, Michigan

SUMMARY

The results of an experimental and analytical evaluation of ceramic turbine tip shrouds within a small turbine engine operating environment are presented. The ceramic shrouds were subjected to 1001 cycles between idle and high power and steady-state conditions for a total of 57.8 engine hr.

Posttest engine inspection revealed mud-flat surface cracking, which the authors attributed to microcracking under tension with crack penetration to the ceramic- and bond-coat interface. Sections and micrographs tend to corroborate the thesis.

The engine test data provided input to a thermomechanical analysis to predict temperature and stress profiles throughout the ceramic gas-path seal. The analysis predicts cyclic thermal stresses large enough to cause the seal to fail. These stresses are, however, mitigated by inelastic behavior of the shroud materials and by the microfracturing that tensile stresses produce. Microfracturing enhances shroud longevity during early life but provides the failure mechanism during extended life when coupled with the time-dependent inelastic materials effects.

INTRODUCTION

An experimental investigation was conducted to validate the component rig results and the analytical model of the behavior of a ceramic material in the operating environment of a small turbine engine. The bill of material (BOM) turbine tip shrouds, nickel alumide in a honeycomb structure, were replaced by ceramic shrouds. The ceramic shroud has the potential of increasing small turbine-engine efficiency through the use of higher gas-path temperatures or less shroud cooling air, of extending component life through reduced metal temperatures, or of reducing component weight.

Although the ceramic composites offer significant benefits, they are not without certain inherent drawbacks. For instance, the stresses introduced by thermal gradients normally associated with gas-path heating and cooling are compounded by other stresses arising from the thermal expansion differences between the ceramic material and the metallic substrate.

Testing of ceramic material for turbine tip shroud application has generally been limited to rig specimens testing. Some experimental testing has been accomplished in large turbine engines, but little has been done on small engines, such as those in the 4.5-kg/sec (10-lb/sec) airflow class, to verify specimen and analytical models. Some of these results can be summarized by the following works:

(1) Short-period thermal cycling and associated thermal stress are responsible for failures of ceramic coated rods subjected to a Mach 0.3 Jet-A/air burner flame (ref. 1).

(2) For sample sets of 20 ceramic-coated rod specimens and 22 ceramic-coated disk specimens, the standard deviations were large - half the norm. Both data sets were best represented by log-normal distribution functions (ref. 2).

(3) Creep of the ceramic was established experimentally for a variety of configurations and heat treatments. Ceramic creep has a significant effect on thermal stresses (ref. 3).

(4) The effects of thermomechanical loading of ceramic coatings were assessed using three numerical methods, MARC, ADINA-ADINAT, and SINDA-FEATS (ref. 4). The methods produced similar stresses and in all cases were sufficiently high to cause failure of the coatings.

(5) Inelastic behavior of the coating and the substrate were considered (ref. 5). While the ceramic could creep, the inelastic behavior of the substrate and ceramic produced high compressive stresses during and at the end of the cooling cycle (ref. 6). These stresses can cause the ceramic-bond coat interface to fail and, if marginal, the coating can fail upon heatup or during subsequent cycles (refs. 1 and 6).

(6) Testing and modeling of ceramic seal materials and seal configurations produced similar stresses which were all large enough to cause the coatings to fail (ref. 7).

In the work presented herein, the BOM shroud configuration was replaced by an 8-wt % yttria-stabilized zirconia attached to the shroud base metal or substrate by a NiCoCrAlX (Ni, 23-Co, 19-Cr, 14-Al, 2.5-Ta, 1.4-Mn, 0.6-Hf, 0.3-La) bond coat. An experimental evaluation in an engine was conducted with all six of the BOM shroud segments replaced with the ceramic shroud specimens. The engine was operated for 57.8 hr under steady-state conditions and transient conditions of 1001 cycles between idle and high power to evaluate the durability and heat-transfer characteristics of the shrouds. Through this means a comparison of the stress levels estimated from rig and analytical studies could be made.

Data are presented in terms of ceramic shroud temperature profiles at the start and end of testing, typical radial temperature profiles through the

ceramic material, bond coat and substrate during selected transients, and a comparison of BOM and ceramic shroud temperature profiles. Stress level calculations based on these profiles are included. Photographs of the ceramic shrouds before and after testing are also included as are comments on their condition.

APPARATUS

Engine Installation

The ceramic shrouds were installed as six circumferential segments in a small (4.5-kg/sec (10-lb/sec) airflow class) turboshaft engine as the first-stage high-pressure turbine tip shroud (fig. 1). The advanced-design engine used for this investigation is currently in production for military and commercial applications. It is a front-drive, turboshaft engine with an integral particle separator, a single-spool gas generator section consisting of a five-stage axial, a single-stage centrifugal flow compressor; a through-flow annular combustor; a two-stage axial-flow gas generator (high pressure) turbine; and a free two-stage axial-flow power turbine. The engine testing was done in a ground level test facility, at the NASA Lewis Research Center using Jet A fuel. Trace elements of certain metals such as vanadium pentoxide rapidly degrade ceramic coatings. An analysis of the fuel found insignificant amounts of these elements.

A schematic illustration showing a cross section through a typical turbine tip shroud segment is shown in figure 2. Of importance in this figure is the substrate, Haynes-25, part of the BOM configuration, the NiCoCrAlX bond coat (1.0 mm (0.040 in) nominal thickness), and the 8-wt % yttria-stabilized zirconia (also 1.0 mm (0.040 in) nominal thickness). The preparation and application procedures for the substrate, bond coat, and ceramic are described in the section "Seal Fabrication." A photograph of the six shroud segments after application of the ceramic is shown in figure 3.

Instrumentation

The shrouds were impingement cooled on their back sides using compressor discharge air (see fig. 2). Two thermocouples were attached to the back of each segment (fig. 4). The number of thermocouples was limited (1) by the number of leads that could be fed through the structure containing the impingement cooling holes without significantly altering the cooling pattern and (2) by the number of thermocouples leads that could pass through two ports in the combustor outer wall housing to connect to the facility data system.

The hot-side gas path temperature was calculated using compressor-discharge pressure and temperature, fuel flow, combustor efficiency, and cooling and leakage flow estimates.

Seal Fabrication

The general geometric parameters are shown in figure 5. The importance of concave curvature in reducing spallation will become more apparent in the

analysis. In figure 2 the details of the ceramic gas-path seal are illustrated. The Haynes-25 substrate surface was prepared by cleaning and grit blasting. The NiCoCrAlX was then plasma sprayed onto the substrate in a low-pressure environment to a nominal thickness of 1.0 mm (0.040 in).

The results of several-small scale tests at high thermal loadings (refs. 1 to 7), along with the thermal loading of the engine, indicated that a nominal thickness of 1.0 mm (0.040 in) of ceramic material could withstand engine thermal cycling. The component was plasma sprayed, in air, with 8-wt % yttria-stabilized zirconia and heat treated to alleviate NiCoCrAlX strain. Excess material was left to be ground to the engine contour to permit effective rub-free sealing. A schematic representation of the shrouds as installed in the engine after final grinding is shown in figure 6. Variations in the ceramic thickness are due to the fact that the process was not optimized.

PROCEDURE

Transient Cycle Generation

The test operations cycle was represented by 80 sec of operation at high power followed by 80 sec at flight idle power with 1-sec ramps between the two power levels (see fig. 7). The substrate temperature reached equilibrium during the heatup (flight idle to high power acceleration) but did not quite attain equilibrium during the cooldown (high power to flight idle deceleration). Plots of engine speed indicate an overshoot in speed for both heatup and cooldown (fig. 8). These excursions were considered in the calculated gas temperature, but were not detected in the substrate temperature histories as will be discussed under RESULTS AND DISCUSSION.

Cycle Choice

Creep, failure criteria, application, and thermal load affected the choice of operating cycle. The creep experienced by thermal barrier coatings is controlled primarily by the cumulative time at temperature under load and by the rate of temperature change to attain that temperature level. Therefore, it is necessary to cycle the shrouds for a time long enough to reach and maintain that temperature before the cool-down cycle begins (ref. 5).

In earlier work (ref. 2) 22 test samples were cycled in a 0.3 Mach burner. The data were compared with several failure distributions, including Weibull, normal, and log-normal. The test group was most accurately modeled by a log-normal distribution. This implies a decreasing hazard function with increasing time, which is opposite that of a Weibull distribution used in bearing failure theory, where the hazard function increases with time. This was one more reason why 1001 was considered to be a representative number of cycles.

For the seals to be useful for potential engine applications, a relatively large number of cycles had to be tested. The number 1001 appeared as a reasonable compromise between too few cycles and too many (e.g., 10 000).

The engine was limited to a power level less than maximum (~96 percent maximum high rotor speed) to prevent inadvertent trips to idle if the limiting

turbine temperature or high rotor speed were reached during the speed overshoots shown in figure 8. Even with this restriction, gas path temperatures over 1205 °C (2200 °F) were reached during high power operation.

The 12 shroud thermocouples were monitored in real time using an electronic bar graph display to ensure safe engine operation with the ceramic shrouds. In addition, the engine was periodically partially disassembled for visual inspections of the ceramic seals during the course of the program.

RESULTS AND DISCUSSION

Discussions of the experimental and analytical results are divided into the engine test results, consisting of plots of gas-path temperatures and shroud backside temperatures; theoretical results, where the thermal profiles through the shrouds were used to calculate simple stresses; and a materials analysis section describing the posttest observations.

Experimental Results

The engine was operated through 1001 cycles from idle power to high power and back to idle with the ceramic shrouds installed. Counting all the engine time from shroud installation to removal this amounted to 57.8 engine hr. This included initial engine-facility shakedown tests and daily engine-instrumentation health checks. A typical engine acceleration from idle to high power is shown in figure 8(a). The corresponding gas-path temperature and the average of 12 thermocouple readings for the shroud back-side temperature are shown in figure 9(a). Similarly, the engine high-rotor speed and average gas-path and shroud temperatures for deceleration are shown in figures 8(b) and 9(b).

Normalized steady-state shroud back-side temperature after the first and the last (1001) cycles are shown in figure 10. As can be seen in this figure, thermocouples on shroud 6 are somewhat out of agreement with the trend established by the other thermocouples. However, the thermocouples showed no visual or electrical signs of distress under posttest inspection. Possible explanations for this situation include cooling hole blockage, which limited flow to the backside of this shroud, excess coolant bleeds to the hot-gas path, thinner than normal ceramic coating, combustor temperature profile variation, or shroud-to-blade clearance variation from nominal. This problem has not been resolved.

The numerically computed temperature profiles through the substrate, bond coat, and ceramic for engine acceleration and deceleration are shown in figure 11. Figure 9 shows that for acceleration an equilibrium condition was reached in ~40 sec, while for deceleration equilibrium was not quite reached during the cycle. The method used to calculate these profiles is contained in appendix A.

A photograph of the shrouds before installation in the engine is shown in figure 3. Photographs of a shroud after removal from the engine are shown in figure 12. Visual inspection reports after 4, 210, and 739 cycles are contained in appendix B. Comments on the condition of the shrouds after completion of testing are contained in ANALYSIS OF A MATERIALS SECTION, which is to follow.

A comparison of the shroud back-side temperatures for the ceramic and the BOM shrouds after the first cycle for both are shown in figure 13. While on the whole the ceramic temperatures were significantly lower, the opposite was true for such as thermocouples 1, 10, 11, and 12. This lends some credence to the previous hypotheses as to the higher than nominal temperatures in the vicinity of shroud 6. Excluding these thermocouples the difference between the ceramic and the BOM shrouds was approximately 78 °C (140 °F) on the average. The numerically computed radial gradients through the BOM shrouds for an engine acceleration and deceleration are shown in figure 14. A comparison of these radial gradients with those of the ceramic material (fig. 11) shows that the temperatures through the ceramic are lower, testifying to its insulating ability over that of the BOM material.

Theoretical Results

Using the gas temperatures calculated for the high-rotor-speed profiles of figure 8 along with the engine parameters, the heat-transfer coefficients on the hot-gas side can be estimated. The calculation of shroud heat transfer was complicated by an axially driven flow and a periodic, circumferential flow interlaced with radial and secondary flow fields with mass addition. Several things are unknown, such as the effects of secondary flows due to flow over the airfoil, the flow coefficient for a leading-edge geometry with one boundary in motion, the airfoil leading and trailing edge effects, the local velocities (Mach number), heating rates, effects of seal leakage and blade tip coolant discharge, turbulence, etc.

In short, the coefficient was estimated, based on modified pipe flow theory, and more than doubled to investigate the sensitivity of the stresses to the heat transfer coefficient. Values of 1262 and 3154 J/sec-m^2 (400 and 1000 Btu/hr-ft^2) were used. The results were not significantly different for the two heat-transfer coefficients. The models used for the heat-transfer cal- culations were a one-dimensional lumped node model (appendix A) and a two-dimensional ADINAT model (ref. 4).

The models used are illustrated in figure 15. A variable number of elements were used per layer of material, ceramic, bond coat, and substrate for the one-dimensional model (fig. 15(a)). The 6-element (two-dimensional) model with 33 nodal points used an 8-node serendipity element (fig. 15(b)) with 4-Gaussian quadrature points per element situated approximately at 1/3 of the distance from the boundaries. Although a one-dimensional conduction model could have been used for heat transfer, the two-dimensional model was used to be compatible with the thermostress program, ADINA (ref. 4).

The time and temperature histories (fig. 9) were used as input to ADINAT. The base cycle of 80 sec of heating and 80 sec of cooling was followed for one cycle. The properties were interpolated using the time-step Euler backward implicit scheme.

In the thermostress program, elastic behavior was assumed throughout, and the symmetry condition invoked on the model for ADINA. The model was the same as used for the thermal cycle.

Typical thermal profiles though the shroud are illustrated in figure 11 for the thermomechanical heatup and cooldown parts of the cycle. In contrast

to burner rig tests, these profiles indicate a near-zero heat flux for a short time during cooldown; as such, the cooling is more uniform.

Using the thermal profiles generated by ADINAT, the radial, shear, circumferential, and longitudial stresses within the shroud were computed. The longitudinal stresses are illustrated in figure 16 for the heatup and cooldown portions of the test cycle.

For this inelastic behavior case, radial and shear stresses are small, with the radial stresses negligibly small. The significant stresses for this case are the longitudinal and circumferential stresses, which are similar in magnitude. The longitudinal stresses are illustrated in figure 16 for the heatup and cooldown portions of the test. The longitudinal stresses are tensile at the surface during the cooldown portion of the cycle. These produce surface microcracking. Also, the stresses at the ceramic side of the bond coat and ceramic interface are always tensile, a condition leading to microcracking but not necessarily to material failure.

The test results for the ceramic shroud described herein offer proof of performance for all areas except rub tolerance. Since an actual fabrication would probably use a shroud protruding into the gas envelope, rub tolerance could be an important factor. Its importance could be checked by adding a vertical load to the model to determine the locations of the stress risers.

ANALYSIS OF A MATERIAL SECTION

A metallurgical evaluation of a ceramic shroud segment is contained in appendix C. Highlights of the evaluation follow. A typical cross section through one of the ceramic shroud components shows that the ceramic coating thicknesses are not uniform. Figures 17 and 18 present micrographs of such a section. In figure 17(a) the section shows surface cracking. On an average the mud-flat cracks are about 1.5 mm (0.059 in) hexagonally spaced. Such large cracks have probably been preceeded by microfracturing. Figure 18(b) indicates that the cracks tend to penetrate to the bond coat interface where cracking appears to either terminate or, in some instances, spread axially and perhaps circumferentially.

These cracks appear to be responsible for the ability of the shroud to withstand thermal cycling when the elastic analysis produces stresses beyond the rupture limit. Such inelastic behavior also limits the life of the component when, as microfracturing effects become prominent, the structure weakens, and eventually fails.

CONCLUDING REMARKS

Future experimental research work should continue with emphasis on greater ceramic thicknesses, different ceramic application techniques, lower density ceramics, and better definition of the radial temperature and strain profiles through the ceramic shrouds by the use of more thermocouples and implanting of strain gauges.

APPENDIX B

CERAMIC TURBINE TIP SHROUDS TEST PROGRAM
BORESCOPE INSPECTION RESULTS

(A) First Scheduled Inspection - January 19, 1984, after four cycles.
- (1) Fuel nozzles and combustor OK; some soot (black buildup evident, especially around swirl cups. Additional soot buildup evident inside tail-cone and exhaust collector).
- (2) Stage 1 nozzle OK.
- (3) Shrouds ceramic material in excellent condition. No visible sign of wear or use.
- (4) Thermocouple leads intact; no burns of any kind. Cement at shroud support holes (used to route leads to shroud back sides) looked untouched. All straps in place.

(B) Second Scheduled Inspection - January 27, 1984, after 210 cycles.
- (1) Fuel nozzles and combustor OK; no additional soot buildup noted.
- (2) Stage 1 nozzle OK.
- (3) Shroud inspection:
  - (a) A discoloration (blackish darkening) on the leading corner of shroud 5 at the gap next to shroud 4. Looked OK, though, viewed from several angles.
  - (b) A small chip out of the ceramic material on shroud 5. Located in the unblended area on the front-middle edge of shroud 5 at the gap to shroud 4. Size of chip estimated as 1.0 cm^3 (1/16 in^3), at the most.
  - (c) All other shrouds OK; some sign of use was visible.
- (4) Thermocouple leads good; some cracking of the cement used to seal the leads as they go through the tubes to the shroud back sides at shroud 2.

(C) Third and Last Scheduled Inspection - February 3, 1984, after 739 cycles
- (1) Fuel nozzles and combustor OK.
- (2) Stage 1 nozzle OK.
- (3) Shroud inspection:
  - (a) The discoloration, noted in (B3a) was not observed in this inspection. No explanation; possibly a shadow or a carbon deposit burned clean.
  - (b) The small chip, noted in (B3b), was not further deteriorated.
  - (c) A small chip out of the ceramic material on shroud 2, located in the unblended area on the front edge of shroud 2 at the gap to shroud 1. Size of chip estimated as 1.0 cm^3 (1/16 in^3). As the chip on shroud 5 has been, it was triangular in shape.
  - (d) A very-small chip out of the ceramic material on shroud 3, located in the unblended area on the front middle edge of shroud 3 at the gap to shroud 4. Size of chip estimated as 1.6 by 0.8 by 0.8 mm (1/16 by 1/32 by 1/32 in), at the most, and was barely visible.
  - (e) Discolorations observed at five of the six gaps between the shrouds. Dirty (blue-blackish) tint seen on the metal leading edge at all gaps except the gap between shrouds 3 and 4.

(f) A shiny area on the metal leading edge of shroud 1. The area was about 19.1 mm (3/4 in) long and extended into half the metal width between position indicators a and b. (See fig. 6.)
(g) All other shrouds looked OK; additional sign of use was visible as overall darkening.

(4) Thermocouple leads looked OK; cement cracking noted in (B4) again observed, no further deterioration.

APPENDIX C

CERAMIC SHROUD - METALLURGICAL EVALUATION

A metallographic study (by General Electric Co. under contract to Lewis) found that, although the ceramic shroud specimen looked exceptionally good after 1001 thermal cycles (i.e., no detectable errosion or deterioration) in the engine test, a considerable amount of cracking was evident.

Macroscopic Observations

In this evaluation, one shroud (shroud 6) and a typical cross section were metallographically examined. The front and back surfaces of a typical shroud are shown in figure 12, which indicates a reasonably smooth surface without visible defects. Some slight erosion was evident, along with a small amount of 8-wt % yttria-stabilized zirconia ceramic darkening. Macroscopic observations (figs. 17 and 18) (at 32x) showed cracking in the bond coat region along the trailing edge (fig. 18(a)), which extends back into the ceramic flow path surface. Some ceramic cracking was also evident along the leading edge (fig. 17(b)), along with some surface microfracturing (fig. 17(a)). The right end of the shroud showed both vertical and bond-line cracking (fig. 18(b)).

The degree of cracking around the outer perimeter was measured. Of the total perimeter length of 24.4 cm (9.6 in), 0.9 cm (3.6 in), or ~37.5 percent was cracked.

Metallographic Observations

Shroud 6 was sectioned as shown in figure 19. Metallographic observation of the sectioned shroud indicates the bond coat thickness to be 1.14 to 1.27 mm (0.045 to 0.050 in) thick. The sprayed bond coat in the areas adjacent to the leading edge and trailing edge frame (fig. 20) were of low density, about 50 percent dense. Vertical cracking was also evident in the bond coat. Also noted was the presence of a "cooling" hole through the substrate into the bond coat. This hole does not extend into the ceramic top coat.

The ceramic top coat is about 0.76 to 0.98 mm (0.030 to 0.039 in) thick. The thickness was probably closer to 1.27 mm (0.050 in) before engine grind. Cracking of the bond coat extended almost 1.9 mm (0.075 in) from trailing to the leading edge and 12.7 mm (0.500 in) from right to left end.

Additional Metallurgical Studies

Pretest and posttest microstructures of the plasma sprayed coatings (yttria-stabilized zirconia and NiCoCrAlX) on the engine shroud segments were examined. (Section locations are given in fig. 21.)

The pretest micrograph (fig. 22(a)) was examined on a quality control specimen that was not run in the engine. The micrograph reveals some vertical cracking which provides strain relief.

Examination of posttest ceramic coating microstructure (figs. 22(b) and (c)) revealed extensive segmentation, commonly called mud-flat cracking, and some local areas of lateral cracking and large porosity. Apparently, densification of the ceramic occurred. Caution must be exercised here, however, as observed microstructures are very dependent on metallographic polishing methods. The metallic bond layer exhibited considerable porosity, predominatly due to pullout during metallographic polishing which was optimized to reveal the ceramic microstructure. The extensive porosity noted next to the leading and trailing edges was due to the geometry of the part not having been optimized for plasma spray coating. No evidence of any significant oxidation or β-phase (NiAl) depletion on the NiCoCrAlX bond layer was noted. Variations in the thickness of the metallic and ceramic layers found in sections AA and BB are due to impression of the process.

REFERENCES

1. McDonald, G.; and Hendricks, Robert C.: Effect of Thermal Cycling on ZrO_2-Y_2O_3 Thermal Barrier Coatings. NASA TM-81480, 1980.

2. Hendricks, R.C.; and McDonald, G.: Assessment of Variations in Thermal Cycle Life Data of Thermal-Barrier-Coated Rods. Thin Solid Films, vol. 84, 1981, p. 105.

3. Hendricks, Robert C.; McDonald, Glenn; and Mullen, Robert L.: The Effect of Annealing on the Creep of Plasma-Sprayed Ceramics. Ceram. Eng. Sci. Proc., vol. 4, no. 9-10, Sept.-Oct. 1983, pp. 819-827.

4. Hendricks, R., et al.: Thermomechanical Loading of Multilayered Cylindrical Geometries in Thermal Cycling from 300 to 1300 K. Presented at the ASME/JSME Thermal Engineering Joint Conference, Honolulu, Hawaii, March 20-24, 1983.

5. Padovan, J., et al.: Plastic Flow of Plasma Sprayed Ceramics. Proc. International Symposium on Plastic Deformation of Ceramic Materials, Plenum, NY, 1983, pp. 473-485.

6. Padovan, J., et al.: High Temperature Thermomechanical Analysis of Ceramic Coatings. J. Thermal Stresses, vol. 7, no. 1, 1984, pp. 51-74.

7. Padovan, J., et al.: Thermomechanical Analysis of Ceramic Gas-Path Seals. Ceram. Eng. Sci. Proc., vol. 5, no. 7-8, July-Aug. 1984.

8. Incropera, Frank P.; and DeWitt, David P.: Fundamentals of Heat Transfer. John Wiley and Sons, 1981, pp. 146-165, 214-229.

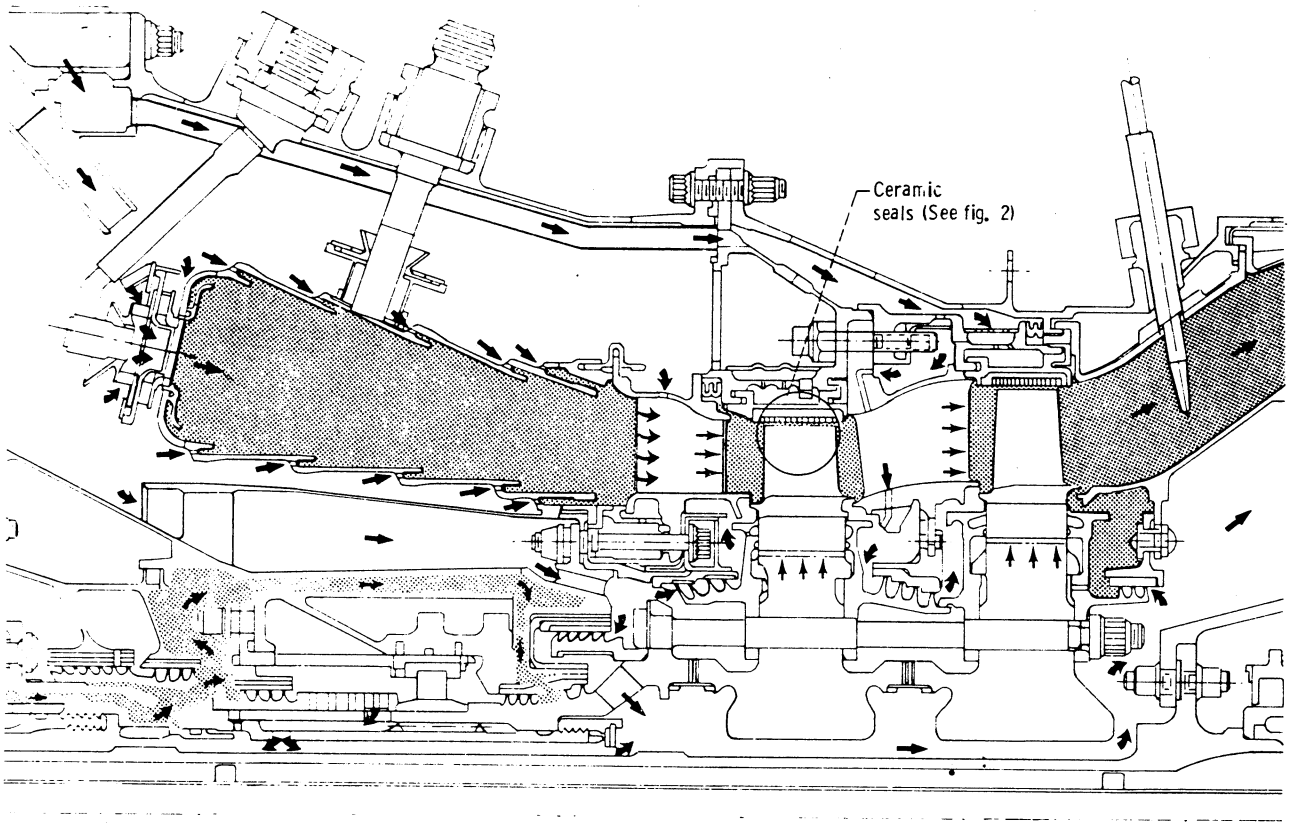

Figure 1. - Engine hot section schematic.

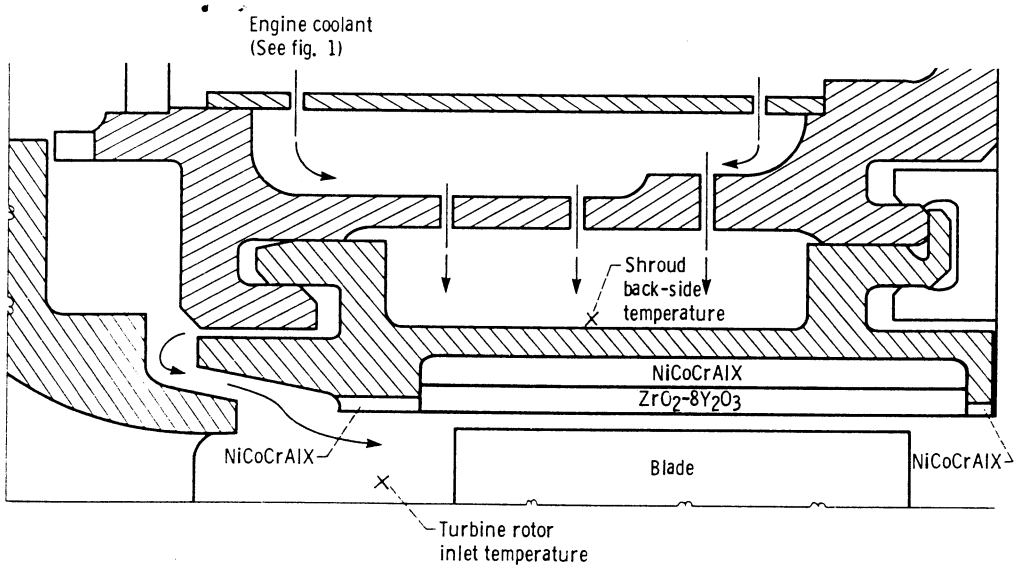

Figure 2. - Schematic of ceramic seal.

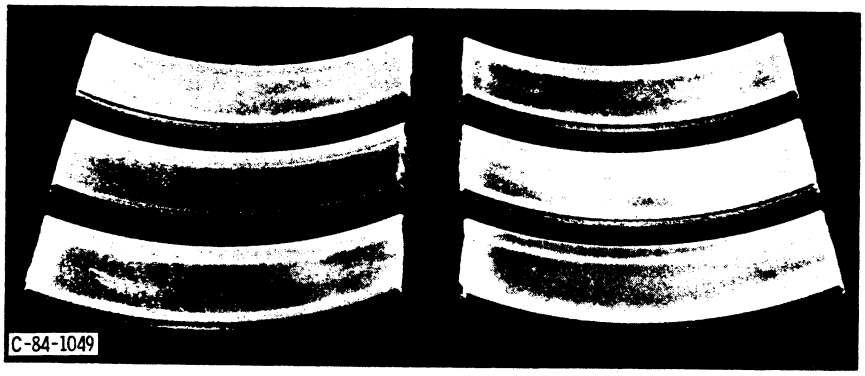

Figure 3. - Shroud segments after plasma spraying.

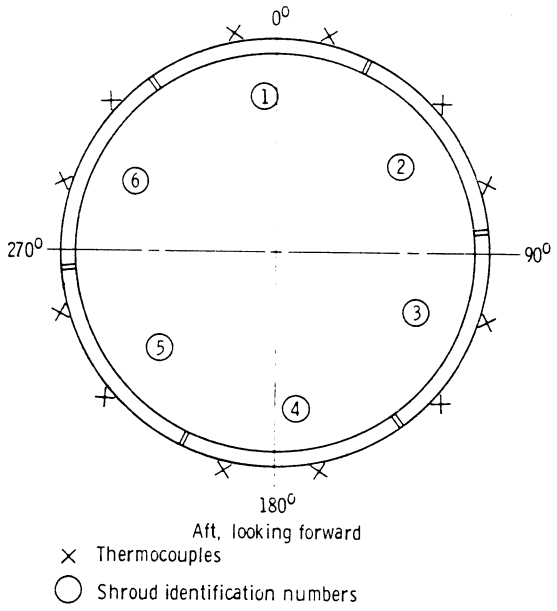

Figure 4. - Position of thermocouples on turbine tip shrouds.

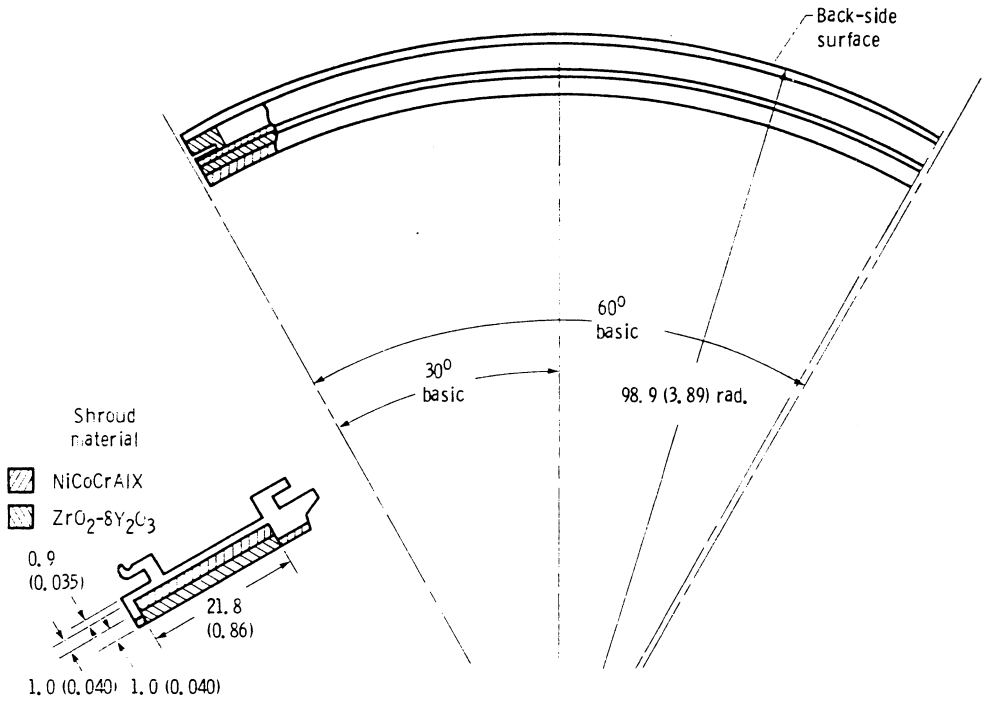

Figure 5. - Shroud general geometric parameters. (Dimensions are in millimeters (inches).)

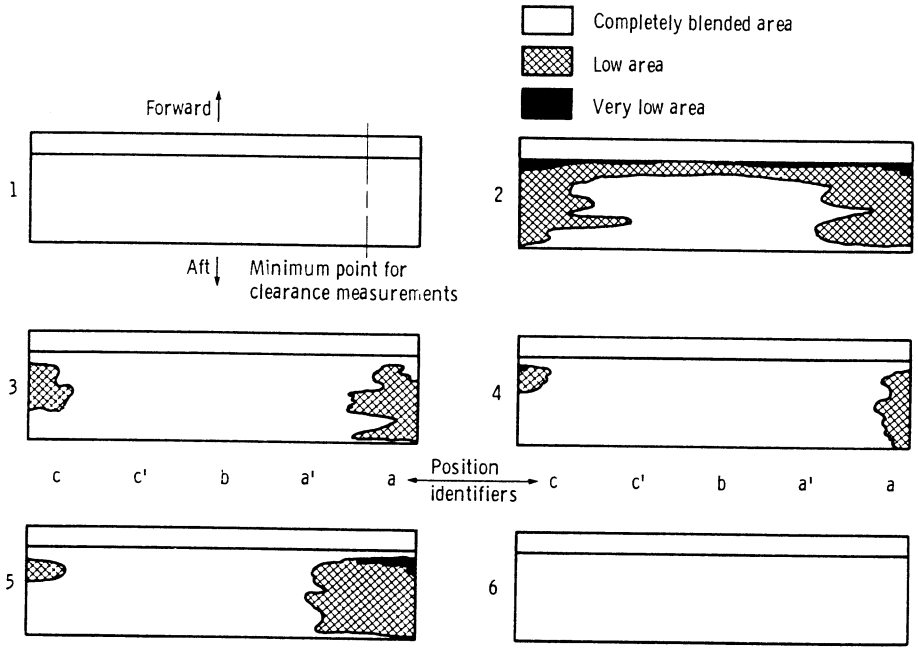

Figure 6. - Schematic of ceramic shroud thicknesses as installed in engine after final grinding.

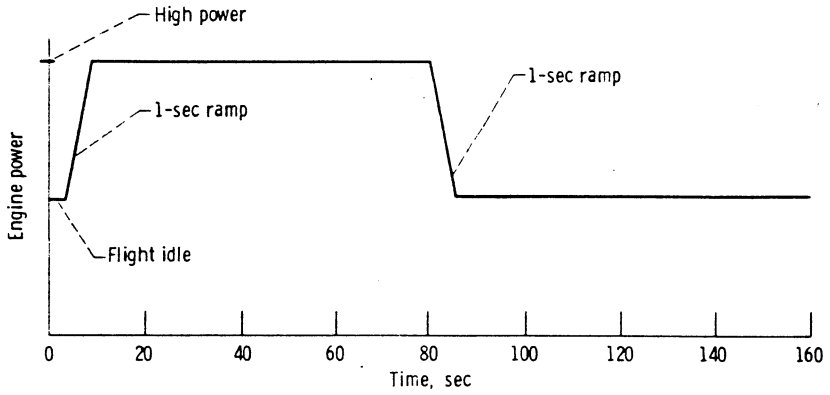

Figure 7. - Typical engine transient cycle.

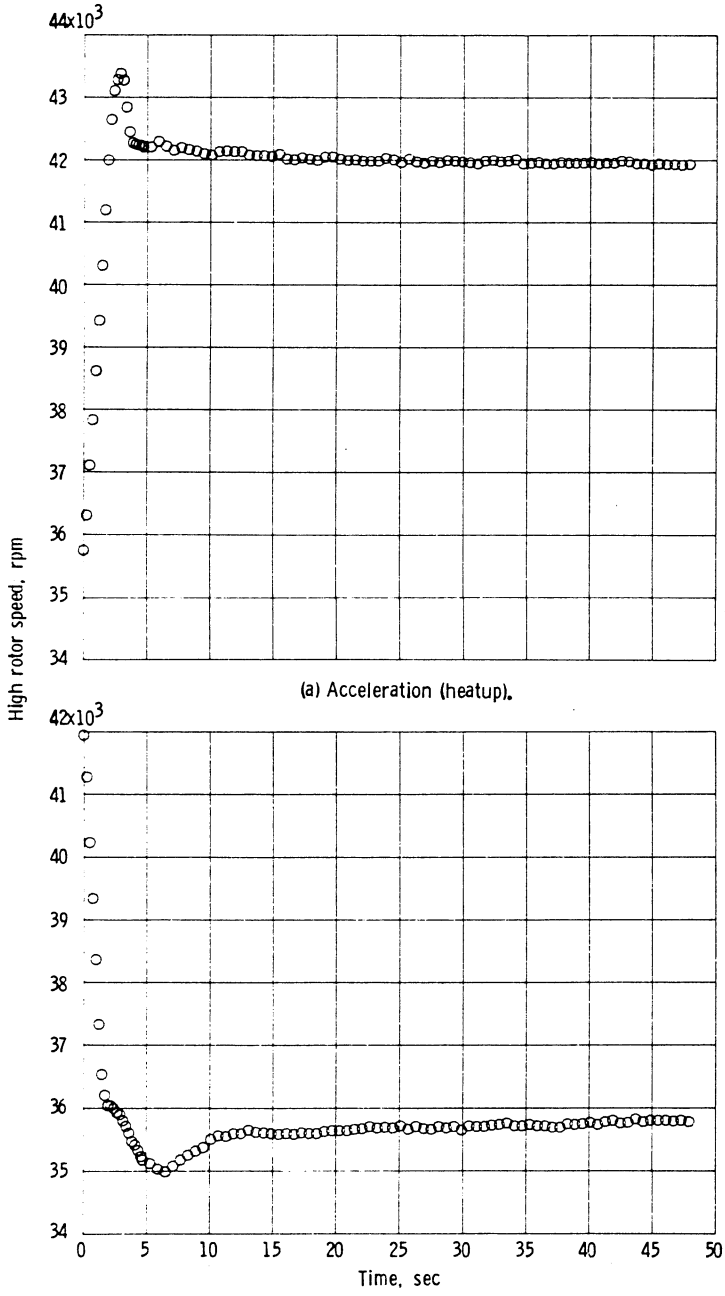

(a) Acceleration (heatup).

(b) Deceleration (cooldown).

Figure 8. - High rotor speed variation with time.

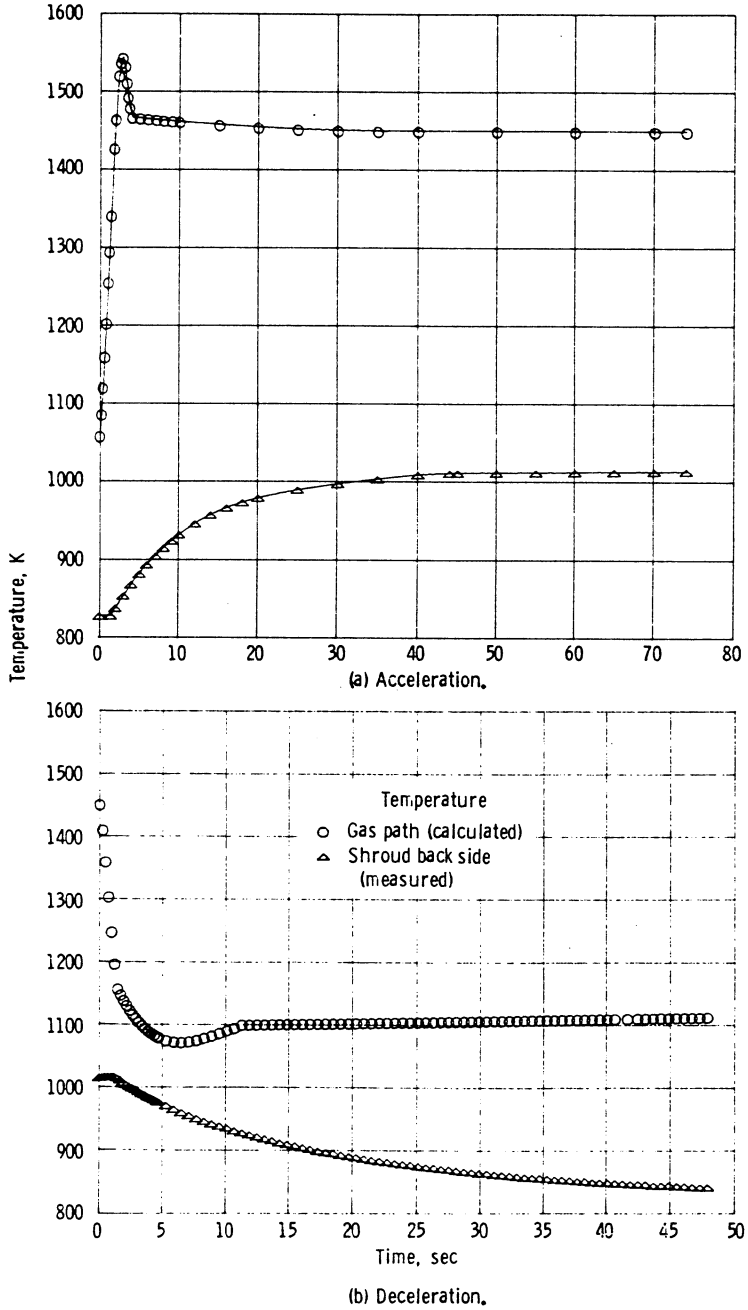

Figure 9. - Average shroud back-side temperature and gas-path temperature variation with time.

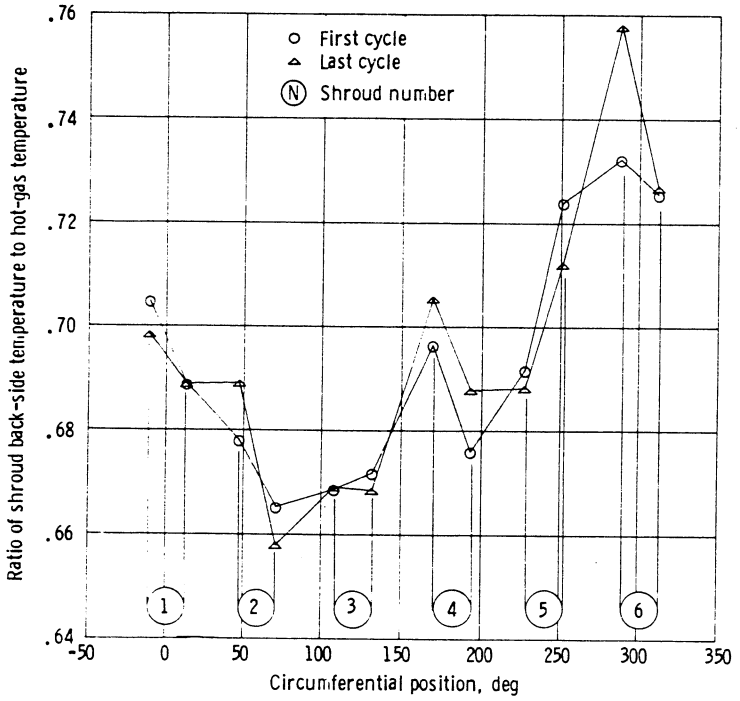

Figure 10. - Normalized shroud back-side temperatures at high power for first and last (1001) cycles.

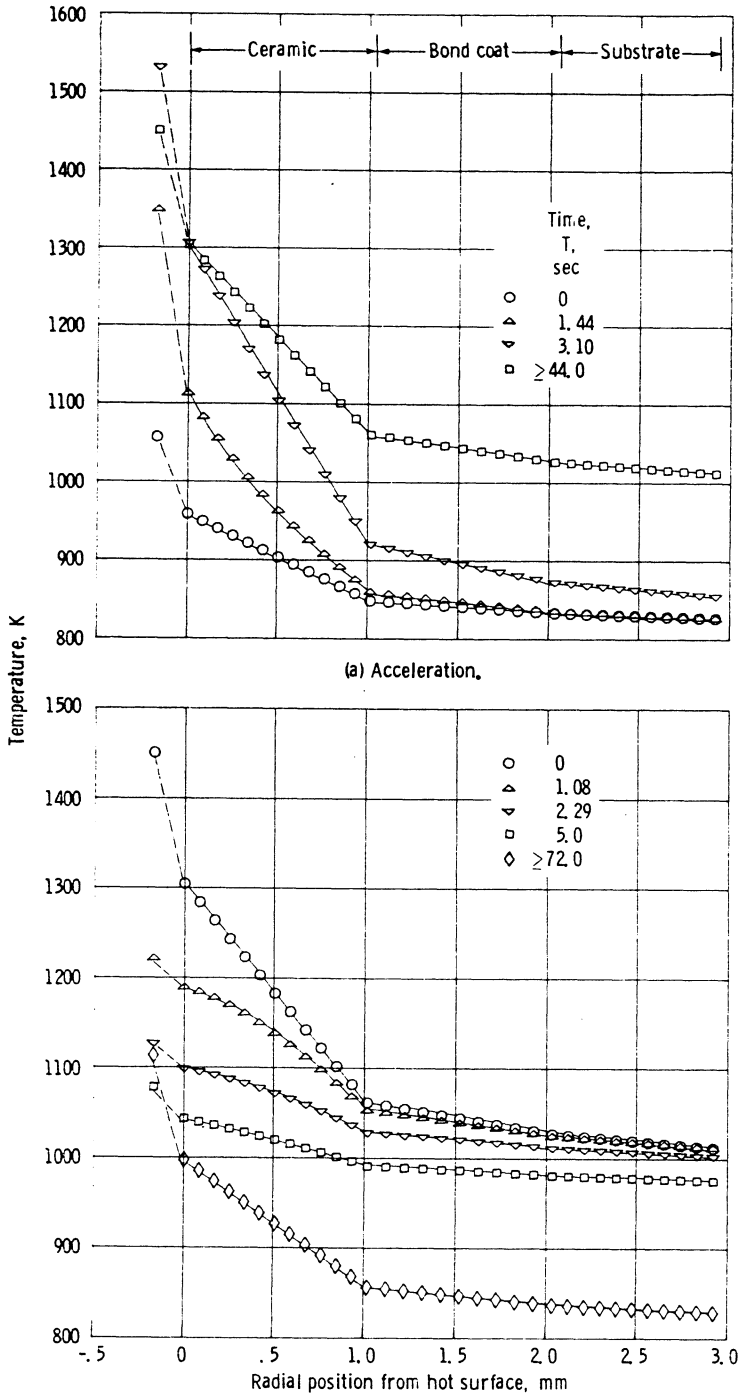

Figure 11. - Variation of shroud temperature profile with time.

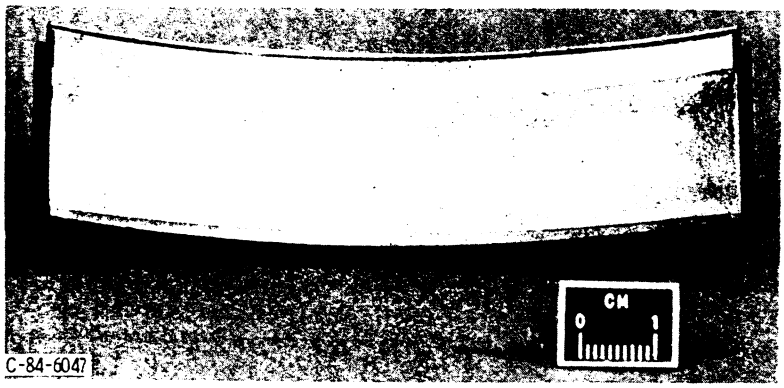

(a) Hot-gas side.

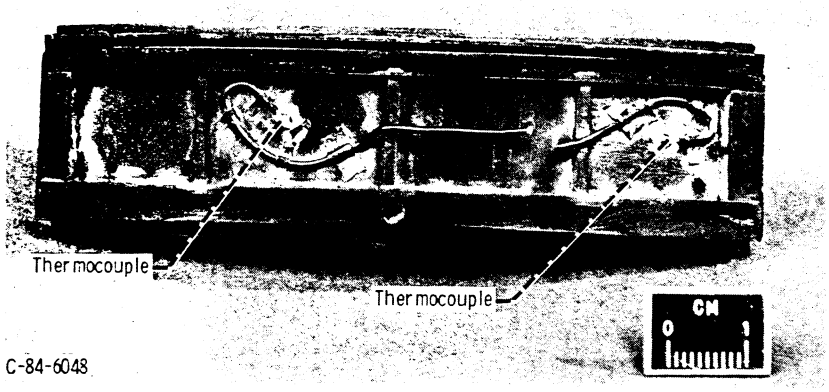

(b) Backside.

Figure 12. - Shroud segment after 1001 cycles.

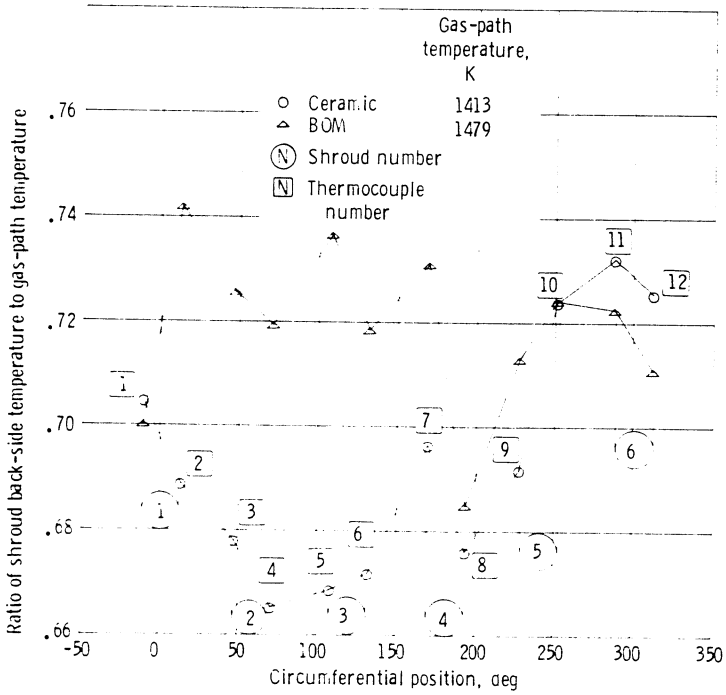

Figure 13. - Comparison of ceramic and bill of material (BOM) shroud back-side temperatures at high power after one cycle.

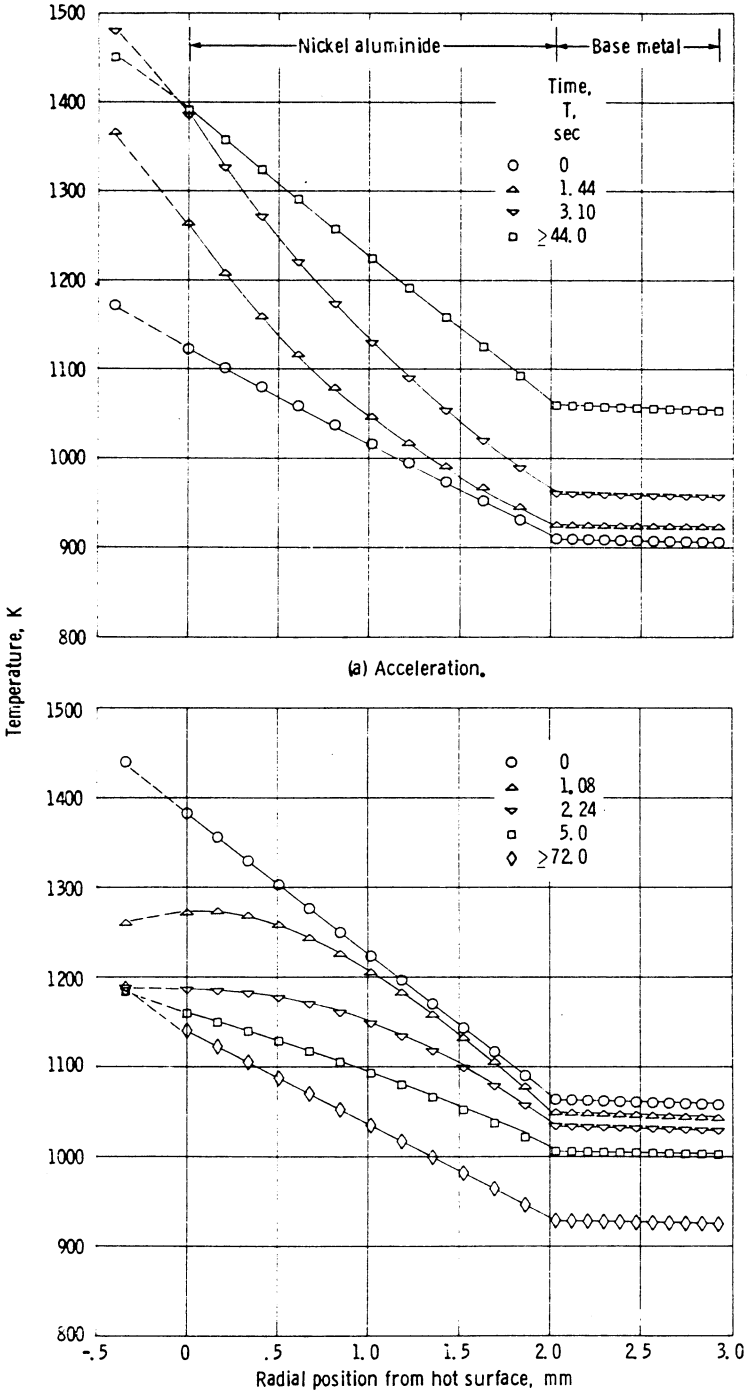

Figure 14. - Variation of bill of material shroud temperature profile with time.

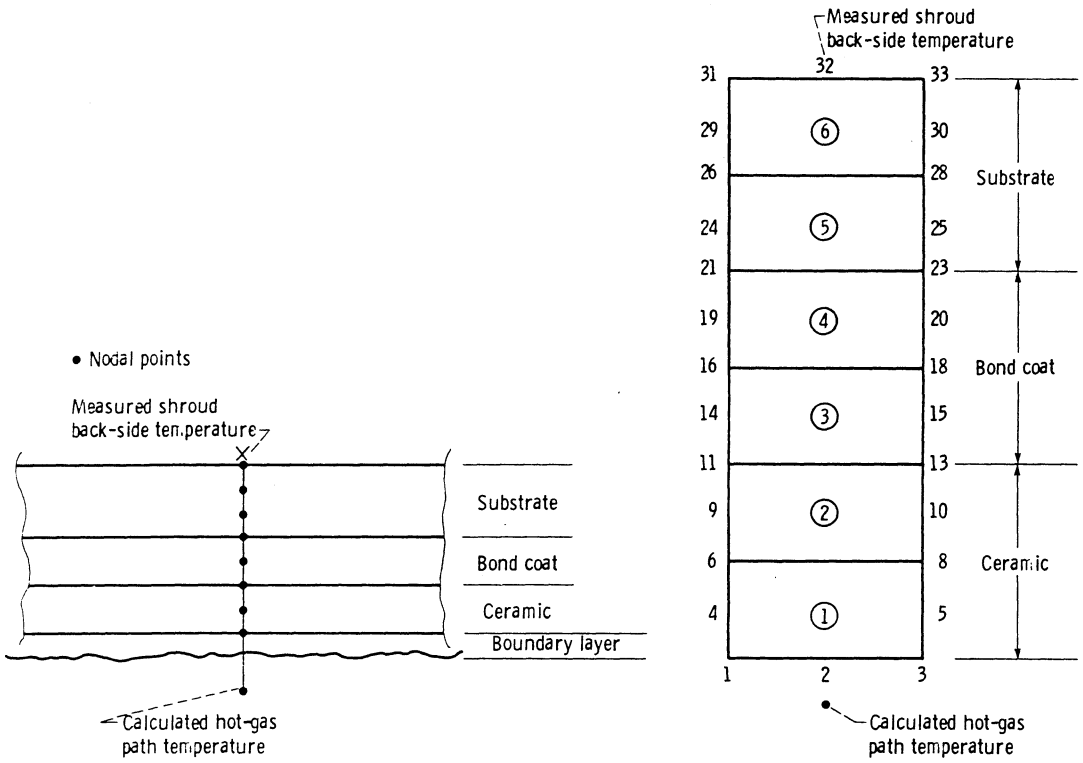

(a) Finite-difference model.

(b) Two-dimensional finite-element model.

Figure 15. - Models used for heat-transfer calculations.

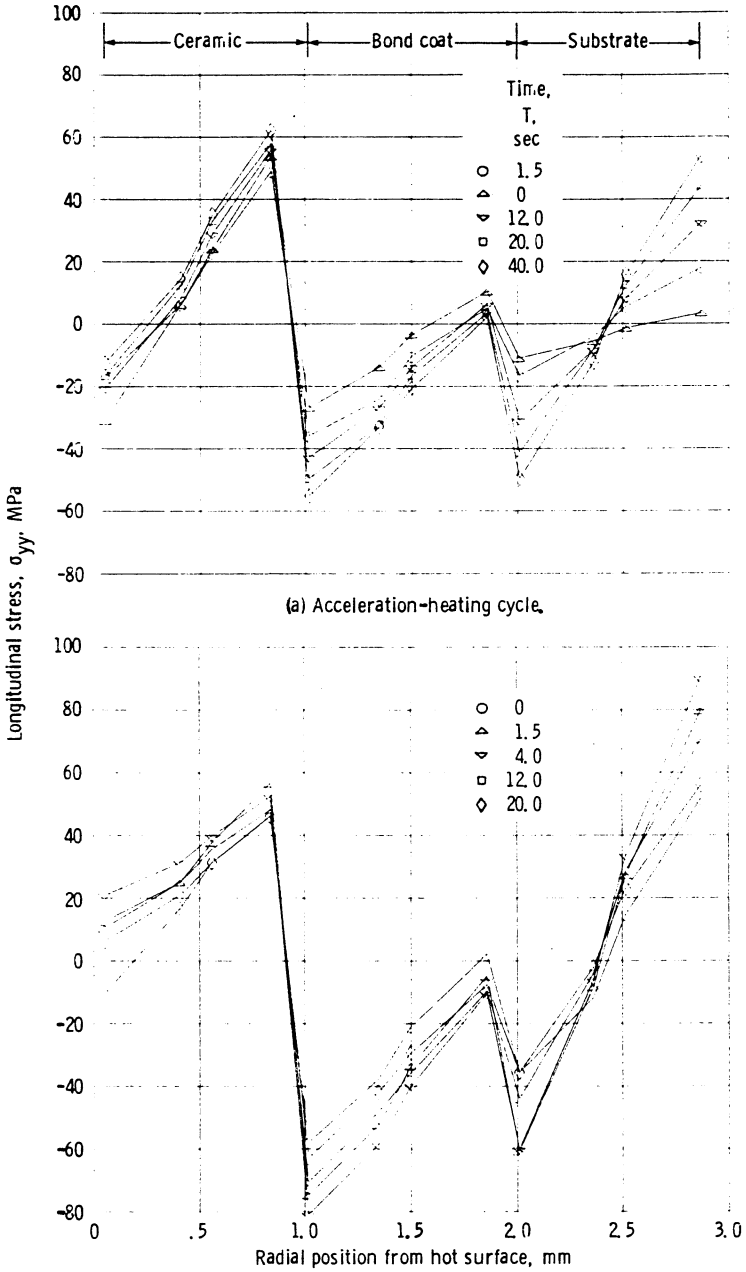

(a) Acceleration-heating cycle.

(b) Deceleration-cooling cycle.

Figure 16. - Shroud longitudinal stress.

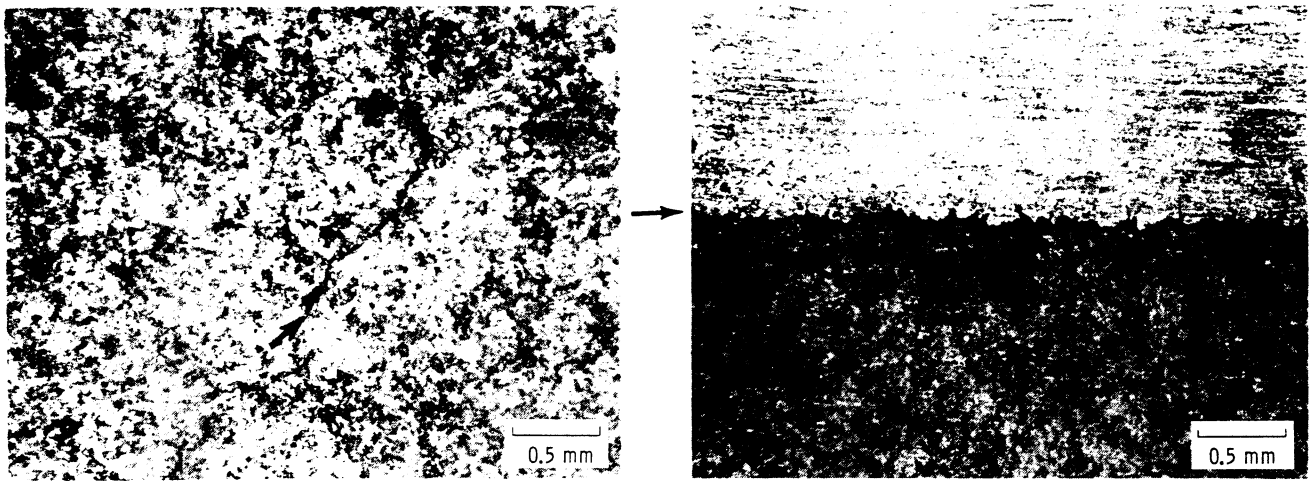

(a) Typical flow path crack.

(b) Ceramic crack leading edge.

Figure 17. - Micrographs of ceramic shroud section - flow path and leading edge.

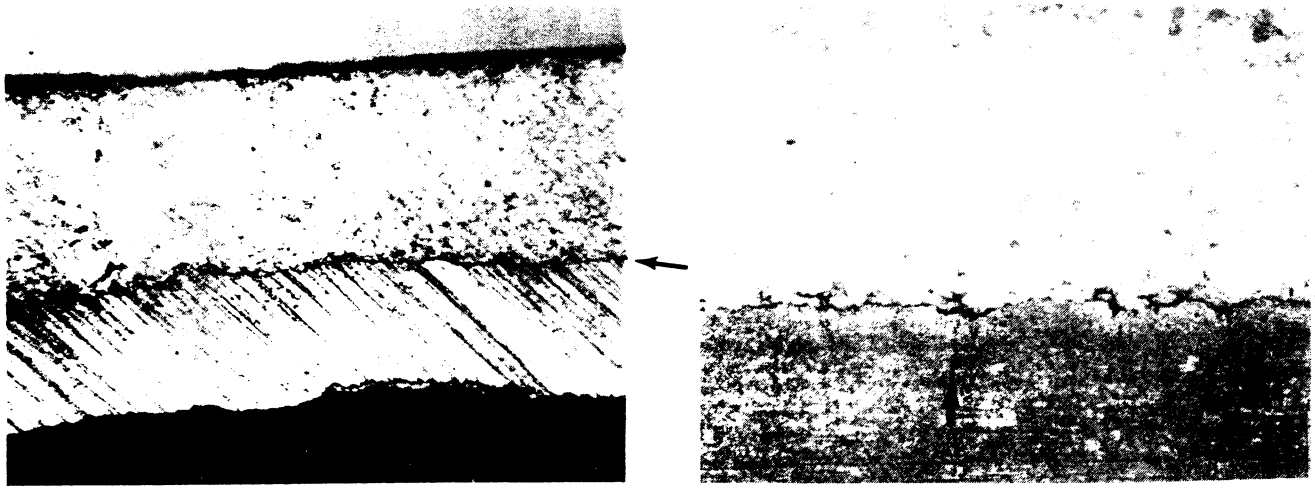

(a) Ceramic and frame crack trailing edge.

(b) Right end bond line and vertical crack.

Figure 18. - Micrographs of ceramic shroud section - trailing edge and right end.

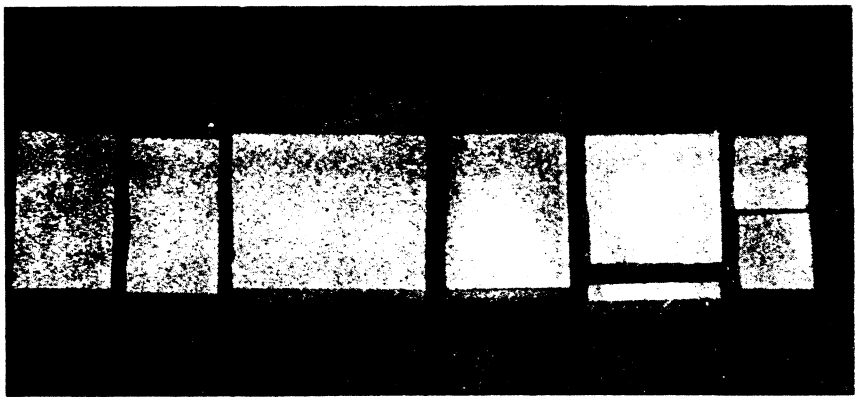

Figure 19. - Shroud sections.

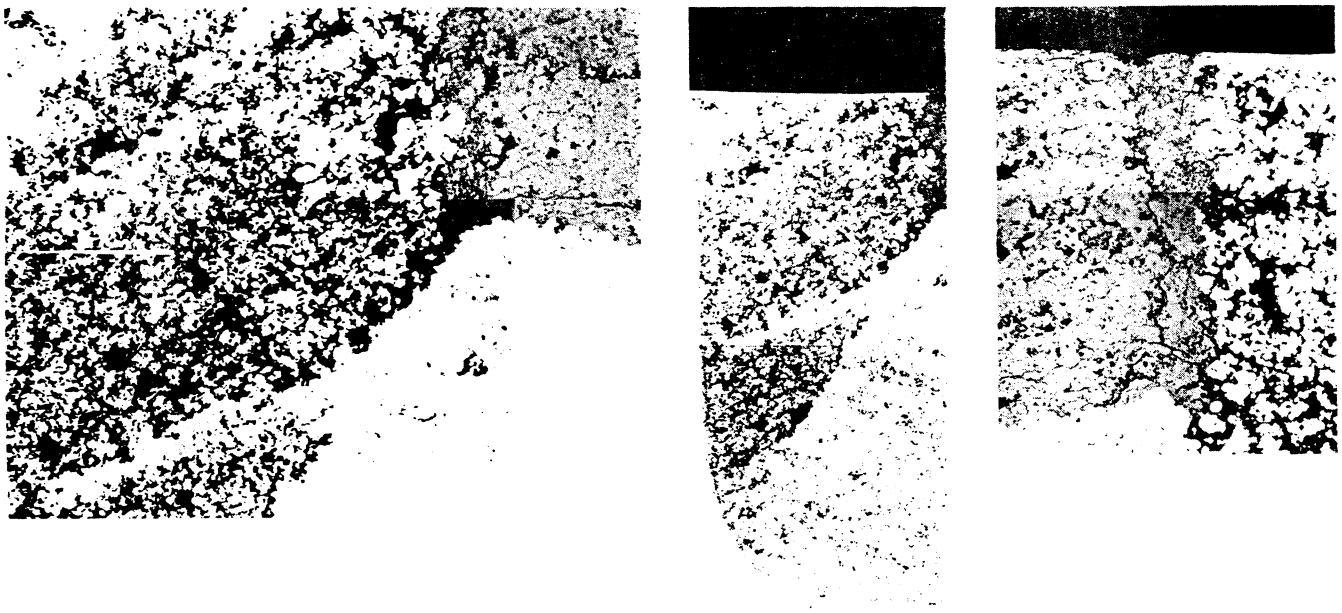

Figure 20. - Low density in bond coat adjacent to leading-edge and trailing edge frames.

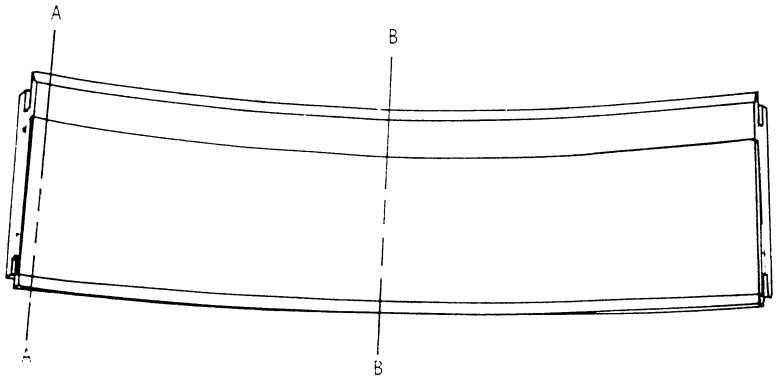

Figure 21. - Metallographic sectioning locations.

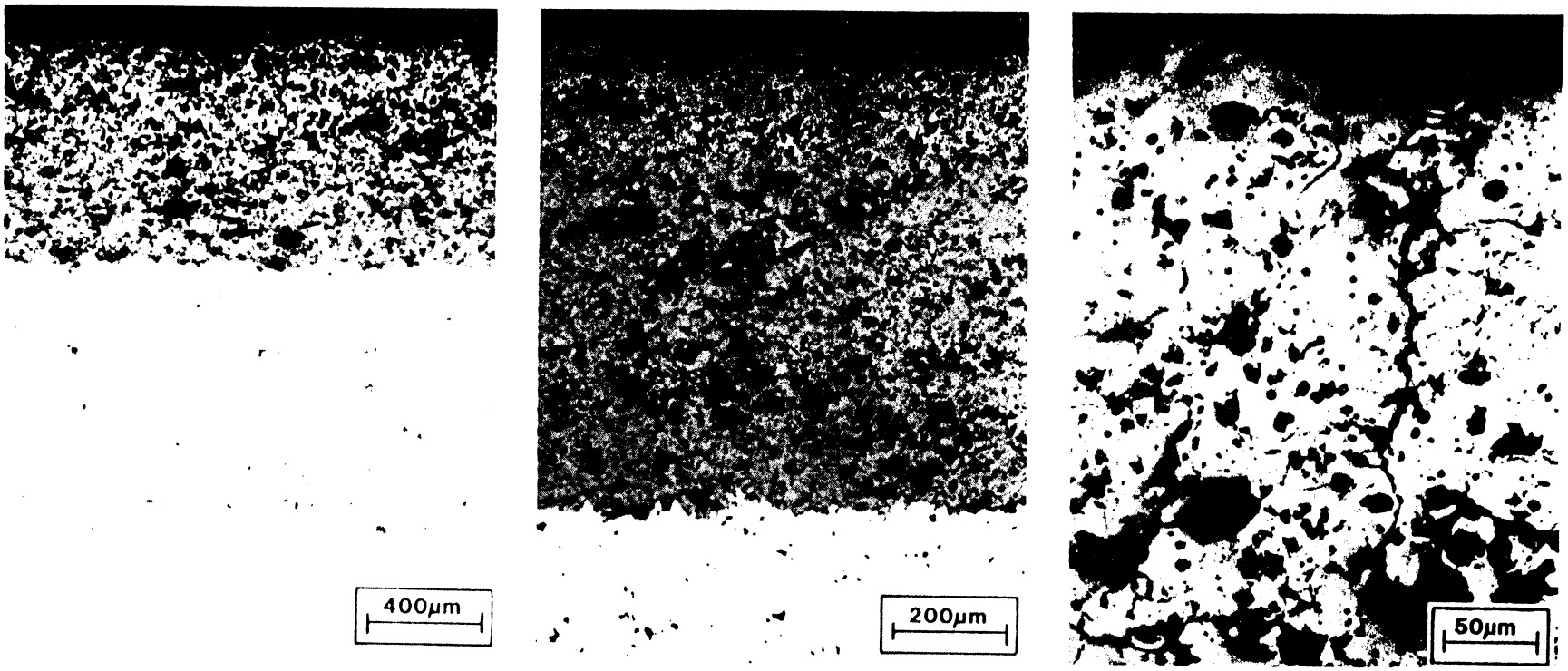

(a) Pretest microstructure; cross section B-B.

Figure 22. - Plasma-sprayed shroud seal. (See fig. 21 for cross-section positions.)

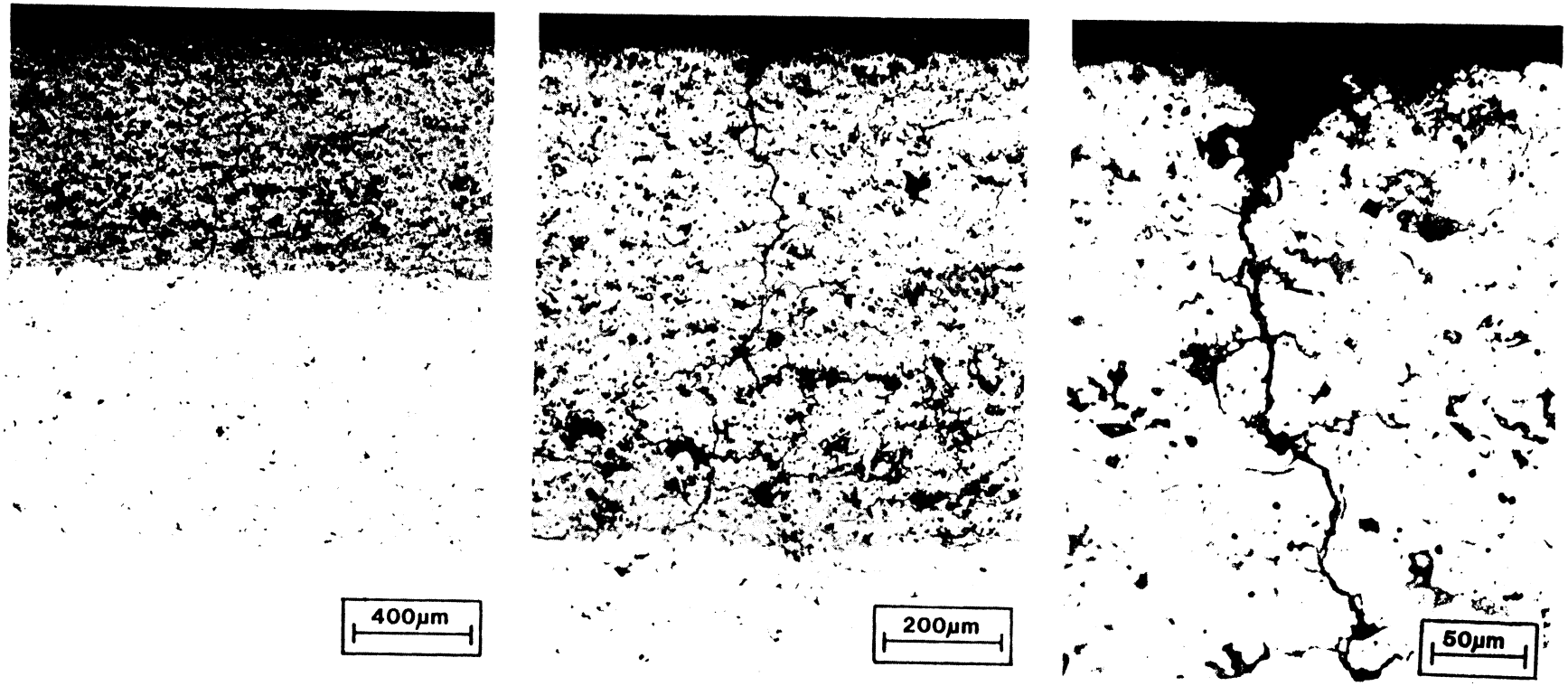

(b) Posttest microstructure; cross section A-A.

Figure 22. - Continued.

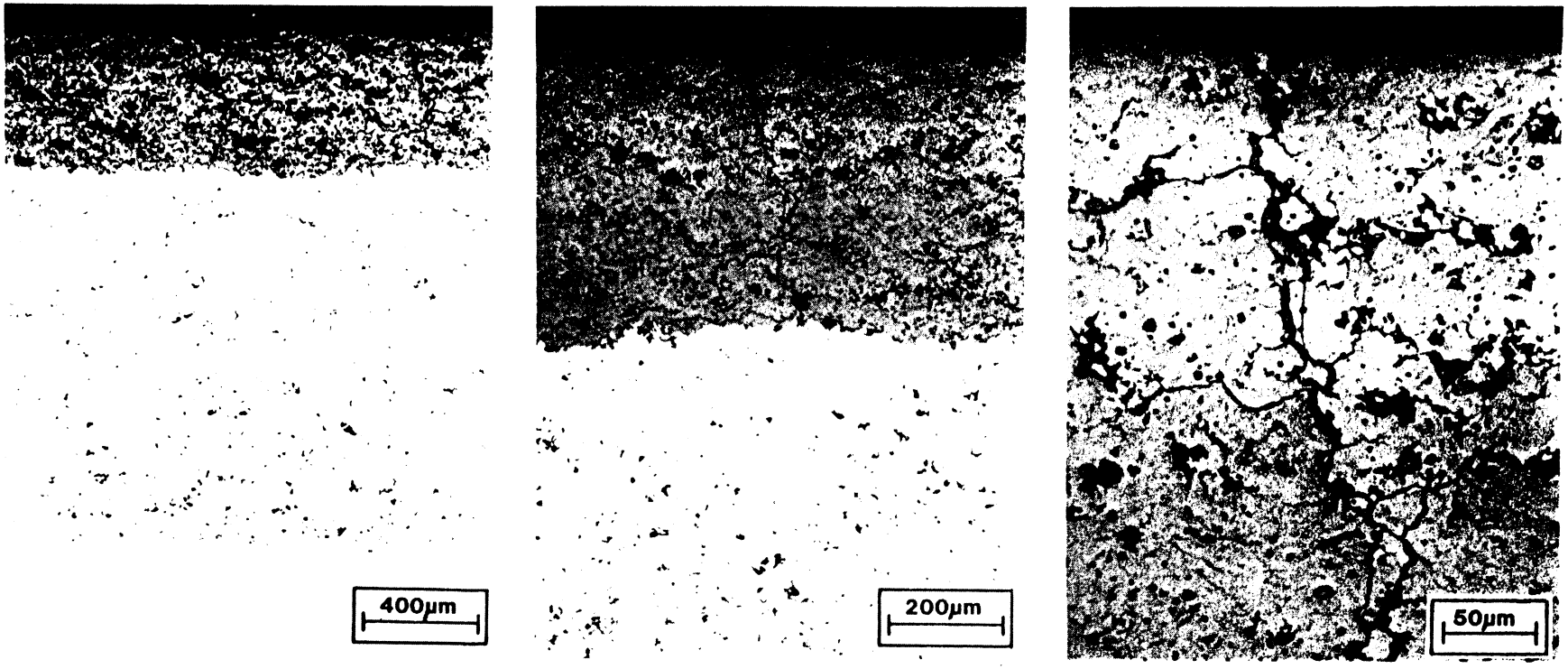

(c) Posttest microsturcture; cross section B-B.

Figure 22. - Concluded.

1. Report No. NASA TM-86881 USAAVSCOM-TR-C-19	2. Government Accession No.	3. Recipient's Catalog No.

4. Title and Subtitle

Experimental and Analytical Study of Ceramic-Coated Turbine-Tip Shroud Seals for Small Turbine Engines

5. Report Date

January 1985

6. Performing Organization Code

505-40-5A

7. Author(s)

T.J. Biesiadny, G.E. McDonald, R.C. Hendricks, J.K. Little, R.A. Robinson, G.A. Klann, and Eliot Lassow

8. Performing Organization Report No.

E-2343

10. Work Unit No.

9. Performing Organization Name and Address

NASA Lewis Research Center and Propulsion Laboratory
U.S. Army Research and Technology Laboratories (AVSCOM)
Cleveland, Ohio 44135

11. Contract or Grant No.

13. Type of Report and Period Covered

Technical Memorandum

12. Sponsoring Agency Name and Address

National Aeronautics and Space Administration
Washington, D.C. 20546 and U.S. Army Aviation
Systems Command, St. Louis, Mo. 63120

14. Sponsoring Agency Code

15. Supplementary Notes

T.J. Biesiadny, G. McDonald, R.C. Hendricks, and J.K. Little, NASA Lewis Research Center; R.A. Robinson and G.A. Klann, Propulsion Laboratory, AVSCOM Research and Technology Laboratories, Lewis Research Center, Cleveland, Ohio; Eliot Lassow, Howmet Turbine Components Corporation, Whitehall, Michigan.

16. Abstract

The results of an experimental and analytical evaluation of ceramic turbine tip shrouds within a small turbine engine operating environment are presented. The ceramic shrouds were subjected to 1001 cycles between idle and high power and steady-state conditions for a total of 57.8 engine hr. Posttest engine inspection revealed mud-flat surface cracking, which the authors attributed to microcracking under tension with crack penetration to the ceramic- and bond-coat interface. Sections and micrographs tend to corroborate the thesis. The engine test data provided input to a thermomechanical analysis to predict temperature and stress profiles throughout the ceramic gas-path seal. The analysis predicts cyclic thermal stresses large enough to cause the seal to fail. These stresses are, however, mitigated by inelastic behavior of the shroud materials and by the microfracturing that tensile stresses produce. Microfracturing enhances shroud longevity during early life but provides the failure mechanism during extended life when coupled with the time-dependent inelastic materials effects.

17. Key Words (Suggested by Author(s))	18. Distribution Statement
Engine tests; Ground tests; Ceramics; Ceramic bond; Turboshaft	Unclassified - unlimited STAR Category 07

19. Security Classif. (of this report)	20. Security Classif. (of this page)	21. No. of pages	22. Price*
Unclassified	Unclassified		

*For sale by the National Technical Information Service, Springfield, Virginia 22161